atoms

MDPI

Article

State-Selective Single-Electron Capture from H_2O at Low Collision Energies Using the Classical Trajectory Monte Carlo Method

James A. Perez * and Josh A. Muller

Physics Department, Luther College, Decorah, IA 52101, USA
* Correspondence: perezjam@luther.edu; Tel.: +1-563-387-1629

Abstract

A three-body classical trajectory Monte Carlo method is used to investigate state-specific electron capture from H_2O by highly charged ions. The radial and momentum distributions of the target electron are modeled using a one-center molecular orbital wave function. Total single-electron capture cross sections, as well as cross sections for capture into specific *nl*-states, are calculated for the highly charged ion projectiles, C^{6+}, N^{7+}, Ne^{10+}, and Ar^{18+}, at relative collision energies ranging from 0.01 keV/amu to 50 keV/amu. Comparisons of relative *n*-state capture populations and total single-electron capture cross sections are made with experimental results. The results show a marked improvement in the prediction of relative *n*-states populated, with the overall single-electron single capture cross sections being slightly low compared with experimental values. Overall, this method of calculating *nl*-states of the captured electron appears to be a promising approach for those wishing to model X-ray and Extreme Ultraviolet (EUV) emissions from comets bombarded by solar wind ions, and fusion researchers trying to determine the effects of impurities in Tokomak reactors.

Keywords: single-electron capture; state-specific electron capture; charge exchange; CX; classical monte Carlo method; CTMC; cometary neutrals; H_2O

1. Introduction

Electron capture by highly charged ions from cometary molecules such as H_2O and NH_3, at low collision energies, has been determined to be the primary mechanism for X-ray and Extreme Ultraviolet (EUV) emissions from comets in the vicinity of the Sun [1–6]. This mechanism was first proposed by Cravens [7], and comparisons of models with the measured spectra support this suggestion [8–10].

The cometary X-ray/EUV emission spectrum is primarily the result of electron capture between the cometary neutrals and the fast solar wind heavy ions [9,10]. The solar wind speeds are on the order of 800 km/s (3 keV/amu). The wind is heated and greatly slowed as it enters the bow-shock region of the comet and interacts with the cometary neutrals [11]. The cometary neutrals include H_2O, OH, H, CO, and O_2, with the most prevalent being H_2O. The most abundant minor solar wind species are ions of C, N, O, and Ne, with the most prevalent being O^{6+} [9].

A sound model of state-selective electron capture between heavy ions and cometary neutrals would allow one to indirectly measure the solar wind composition from the X-ray/EUV spectrum. Developing an accurate model has been hampered somewhat by the

Academic Editor: Ioan Schneider

Received: 20 October 2025
Revised: 14 March 2026
Accepted: 6 April 2026
Published: 10 April 2026

inability to establish benchmark theoretical calculations for the capture probability into specific states at the relatively low collision energies necessary. Atomic and molecular orbital basis set expansion methods are applicable and accurate for charge-exchange collisions when ionization to the continuum can be considered negligible. For highly-charged projectiles and low-energy collisions with low-Z targets, the basis sets and computational time become prohibitive. Therefore, classical and semi-classical methods, such as the classical trajectory Monte Carlo (CTMC) method [12] and the multi-channel Landau–Zener (LZ) method [13], have been used to study charge exchange in these collision regimes. Although the LZ method can be used to estimate the state-specific cross sections, it requires input parameters and is not applicable to very strongly coupled systems.

The CTMC method is a parameter-free method that naturally includes angular momentum and the ionization channel. The CTMC method has been used to investigate how low l-state values are populated at low collision energies, in contrast to the statistical distributions expected at intermediate (10–100) keV/amu collision energies [11,14].

In this work, we employ a three-body CTMC method to investigate the n, l state-specific single-electron charge exchange (CX) capture from H_2O by the ions C^{6+}, N^{7+}, Ne^{10+}, and Ar^{18+} at intermediate-to-low (0.01–50) keV/amu collision energies. We provide total single-electron cross sections and partial-capture cross sections in specific n- and nl-states, and we directly compare the CTMC results with experimental measurements. Atomic units are used throughout this paper.

2. Theoretical Method

The CTMC method is used to calculate state-specific cross sections for single-electron capture by C^{6+}, N^{7+}, Ne^{10+}, and Ar^{18+} from the 1B1 and 3A1 orbitals of H_2O, with binding energies of 12.62 eV and 14.74 eV, respectively, at collision energies ranging from 10 eV/amu to 50 keV/amu. The CTMC method applies to strongly coupled systems, such as interactions between highly charged ions and neutral atoms [15,16], at intermediate energies (1–100 keV/amu) where perturbation techniques are invalid and basis set limitations make quantum methods impractical.

The CTMC method usually involves a projectile (bare ion in this work), a target core, and one active electron. The interaction between the projectile ion and the electron and target core is via a Coulomb potential. The potential between the electron and target core is a screened Coulomb potential developed by Garvey et al. based on Hartree–Fock calculations [17]. The electron's position and momentum vectors are initially randomly chosen from a microcanonical distribution,

$$f(\mathrm{r}, p) = \mathrm{k}\delta\left[\mathrm{E}_i - \frac{\mathrm{p}^2}{2\mu} - V(\mathrm{r})\right], \tag{1}$$

where $\mathrm{E_i}$ is the ionization potential and k is a normalization constant, and along with a random eccentricity, they are constrained to be a solution to Kepler's equation. The electron's orbital plane and the impact parameter for the projectile are randomly chosen. The Hamiltonian is set up for the system, and Hamilton's equations of motion are solved to step the system forward in time.

The electron is deemed to be captured if, after an appropriate number of time steps, the electron's energy with respect to the projectile is negative and its energy with respect to the target core is positive. The final binding energy with respect to the projectile, $\mathrm{E_p}$, is used to find the classical principal quantum number, n_c.

$$n_c = q/\sqrt{(2|E_p|)}, \tag{2}$$

where q is the charge of the projectile ion. The final classical angular momentum is calculated using

$$l_C = \left[\left(x\dot{y} - y\dot{x} \right)^2 + \left(x\dot{z} - z\dot{x} \right)^2 + \left(y\dot{z} - z\dot{y} \right)^2 \right], \tag{3}$$

where x, y, and z are coordinates relative to the projectile nucleus. A quantum sublevel is assigned to the captured electron based on these classical values, using the relationships developed by Becker and MacKellar, in which the classical subspace is divided into bins such that the number of bins equals the relative number of quantum states [18]. The classical to quantum relationships are given by

$$\left[(n-1)\left(n - \frac{1}{2} \right) n \right]^{\frac{1}{3}} \leq n_c \leq \left[(n+1)\left(n + \frac{1}{2} \right) n \right]^{\frac{1}{3}}, \tag{4}$$

for the principal quantum number. The angular-momentum quantum number is found using:

$$l \leq l_c \leq l + 1. \tag{5}$$

The binning of the classical angular-momentum values in this way reproduces the correct $2l + 1$ quantal statistical distributions. The capture cross sections are calculated using

$$\sigma_{event} = \left(\frac{N_{events}}{N_{total}} \right) \pi b_{max}^2, \tag{6}$$

where N_{events} is the total number of positive capture events of interest, N_{total} is the total number of simulated collisions or Monte Carlo trials, and b_{max} is the largest impact parameter that can lead to the capture event of interest. The standard error for the cross section given above is

$$\Delta\sigma_{event} = \sigma_{event} \left[\left(N_{total} - N_{events} \right) / N_{total} N_{events} \right]^{\frac{1}{2}} \tag{7}$$

The maximum impact parameter is chosen by trial and error so that the probability of capture at a larger impact parameter is less than 1%. For a sufficient number of Monte Carlo trials, the standard error is proportional to $1/\sqrt{N_{events}}$. For the cross sections reported here, the number of capture events for partial cross sections into specific n, l states ranged from 30 to 80 thousand, and for total cross sections, the minimum number was about 60 thousand for very low-energy collisions.

Charge exchange is highly dependent upon target-projectile phase-space matching, and the success of the CTMC method to study charge-exchange, ionization, and excitation in collisions between ions and hydrogenic atoms has been attributed to the ability to match the classical momentum distribution one obtains after many simulations with the quantum mechanical momentum distribution. For the ground state of hydrogen, the microcanonical distribution shown above yields the exact quantum-mechanical momentum distribution. The radial distribution, however, does not. Once a momentum value has been chosen in the CTMC simulation, the radial distance is chosen to adhere to the conservation of energy, thus placing a classical restriction on the orbital radial values that the quantum radial distribution does not have to obey. The inability to match the quantum mechanical and the classical radial distribution does not seem to have been that important for charge exchange studies at intermediate collision energies (1 keV/amu–100 keV/amu), but at lower energies, it can be expected that the contributions to charge exchange, at large impact parameters, will have a greater influence on the capture cross sections. One of the motivations for the current work is to examine the possibility of extending use of the CTMC method to relatively low collision energies in the range found in the interactions of solar wind ions with cometary neutrals.

For neutral target atoms other than hydrogen, both the momentum and radial CTMC distributions may differ greatly from the quantal distributions. To use the CTMC method to study collisions between bare ions with the water molecule, for example, it is standard practice to assume the electron of interest will come from the oxygen atom, and to set the initial conditions to simulate a 2p electron attached to the target nucleus via an effective charge, with an appropriate binding energy. In Figure 1, we show the CTMC (columns) momentum and radial distribution representing a 2p electron of oxygen that has a binding energy of 12.62 eV, with the effective charge of the oxygen nucleus being $Z = +1$. The quantal distributions (dashed lines) were obtained using the one-center wavefunctions for the 1B1 orbital of water as calculated by Moccia [19]. Moccia calculated wavefunctions for H_2O using the Hartree–Fock–Roothaan method, expanded about a single center, and using Slater-type functions. Both sets of distributions are normalized. One can see that both the classical radial and momentum distributions differ considerably from the quantal counterparts. The CTMC simulation underrepresents the target electron's higher momentum values; this should lead to more captures into lower principal quantum states than would be expected with a purely quantum calculation.

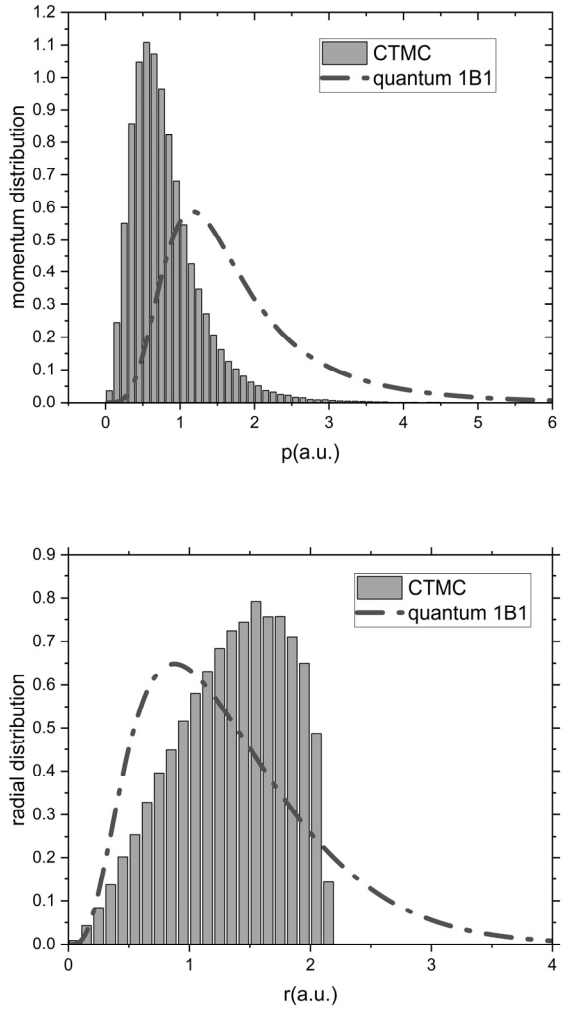

Figure 1. Radial and momentum distributions for the 1B1 orbital in water. The dashed line is the quantum mechanical distributions using Moccia's wavefunction. The columns are the unmodified CTMC distributions assuming a 2p electron centered on an oxygen atom with an effective charge of $Z = +1$. All distributions are normalized.

Several attempts have been made to represent the target system more accurately within the CTMC framework for interactions between bare ions and hydrogen. These alternative

modifications of the method include summing results from microcanonical ensembles with slightly varying binding energies [20], and doing the same with different effective target nuclear charges while keeping the binding energy constant [21].

A promising approach for using the CTMC method to study charge exchange between bare ions and molecules such as water was first undertaken by Otranto and Olson [22]. In that study, they employed the wavefunctions for H_2O orbitals calculated by Moccia. We refer to the distributions calculated with these wavefunctions as the quantum distributions. Otranto and Olson then mapped the CTMC momentum values onto the quantum momentum distributions for each orbital and used a least squares method to find a single effective charge (Z_{eff}) for the target core that would give the best match between the CTMC and quantum radial distribution.

In the present work, we use the method developed by Otranto and Olson to study single-electron capture from water by bare ions for energies ranging from 10 eV/amu to 50 keV/amu. We assume capture only from the 1B1 and 3A1 orbitals with binding energies of 12.62 eV and 14.74 eV, respectively. A least squares approach led to an effective target nucleus charge of $Z_{eff} = 1.6$ for both the 1B1 and 3A1 orbitals. The interactions between the projectile–target nucleus and projectile–electron were Coulomb interactions assuming unscreened charge values. We provide cross sections for total single-electron capture, for capture into the most likely occupied principal quantum states, and for capture into specific angular-momentum states.

It should be noted that our calculated single-electron capture cross sections do not include contributions from double capture followed by Auger emission. Olson and Otranto estimated that this discrepancy led to a 25% underestimation of their calculated single-electron capture cross sections compared to experimental data.

In Figure 2, we show our CTMC radial and momentum distributions as compared with those found using Moccia's orbital wavefunctions. The CTMC still slightly underestimates the contributions from larger orbital distances for the target electrons when compared with the quantum radial distribution.

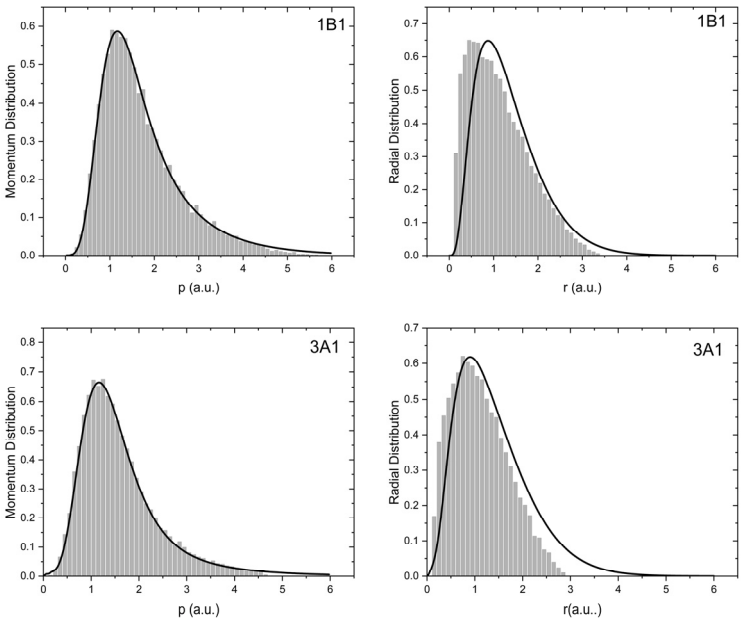

Figure 2. Momentum and radial distributions for the 1B1 and 3A1 orbitals of water. The solid line is the quantum mechanical distributions obtained from the Moccia wavefunctions. The columns are the CTMC distributions used in this work.

The classical microcanonical ensemble usually employed in the CTMC method [Equation (1)], as well as the distributions representing the orbitals used in this work, fundamentally lack the directional symmetries inherent to quantum mechanical distributions. Orientation averaging helps to mitigate these omissions, making the radial and momentum distributions the primary factors in the accuracy of the calculation. This limitation should be particularly relevant at low collision energies, where the specific angular structure of the electron distribution may become a significant factor in capture probabilities.

3. Results

In Figure 3, the results for the total single-electron capture cross sections and the cross sections for capture into the two or three specific n-states that are the main contributors to the total capture cross section are shown. Linear plots were used so as to see the dependence on collision energy that is lost when one uses a log-log plot. For all of the projectiles studied here, we see an increase in the capture cross section when going from collision energies of 10 eV/amu to several keV/amu before decreasing again. At collision energies < 50 keV/amu, we find capture primarily into a single principal quantum number state that follows the $n_f = (q/Z)^{3/4} n_i$ scaling relationship, where q is the charge of the projectile and Z is the effective charge of the target [12]. As the collision energy continues to increase, mixing of states and the population of a broad distribution of quantum states occurs.

This is best shown in Figure 4, which shows the cross sections for capture into specific n- and l-states for the projectile N^{7+} at collision energies of 0.01, 1.0, 12.25, and 100 keV/amu. It can be seen in Figures 3 and 4 that above 10 keV/amu, capture into a broader range of n-states occurs, although the most probable state to capture into remains n = 5 for N^{7+}. State mixing for the occupied angular-momentum states also occurs, as expected. Since the n = 5 state is more likely to be populated, statistically, one would expect capture into $l = 4$ would be most likely, and that is seen for collision energies above 10 keV/amu. At lower collision energies, the captured electron obtains less angular momentum during the interaction and begins occupying lower-angular-momentum states. If Stark mixing were prevalent, about 32% of the captures into the n = 5 state would be into the l = 1 and 2 states.

However, in Figure 4, capture into the $l = 1$ and $l = 2$ states accounted for 27% of the captures at 100 keV/amu, 16% at 12.25 keV/amu, 44% at 1 keV/amu and 67% at 10 eV/amu.

We also compared calculations using this CTMC method with experimental state-selective results for collisions between N^{7+} and H_2O. We wanted to see what improvement, compared with experimental results at relatively low collision energies, could be achieved by using a range of collision energies rather than just one. State-selective capture cross sections were compared with experimental results by Hasan et al. [23]. Total single-electron capture cross sections were compared with experimental results from Greenwood et al. [24]. The experiments by Hasan et al. use a beam of ions colliding with a supersonic target gas. The resulting collisions occur in a plane; thus, to make a more direct comparison between our CTMC calculations and the experimental results, we assumed the collision energies follow a normalized Maxwell–Boltzmann (M-B) distribution with the velocity restricted to the two dimensions of the collision plane, with average energies equal to the reported collision energies of the experimental work, 2 keV/amu and 4.67 keV/amu in this case.

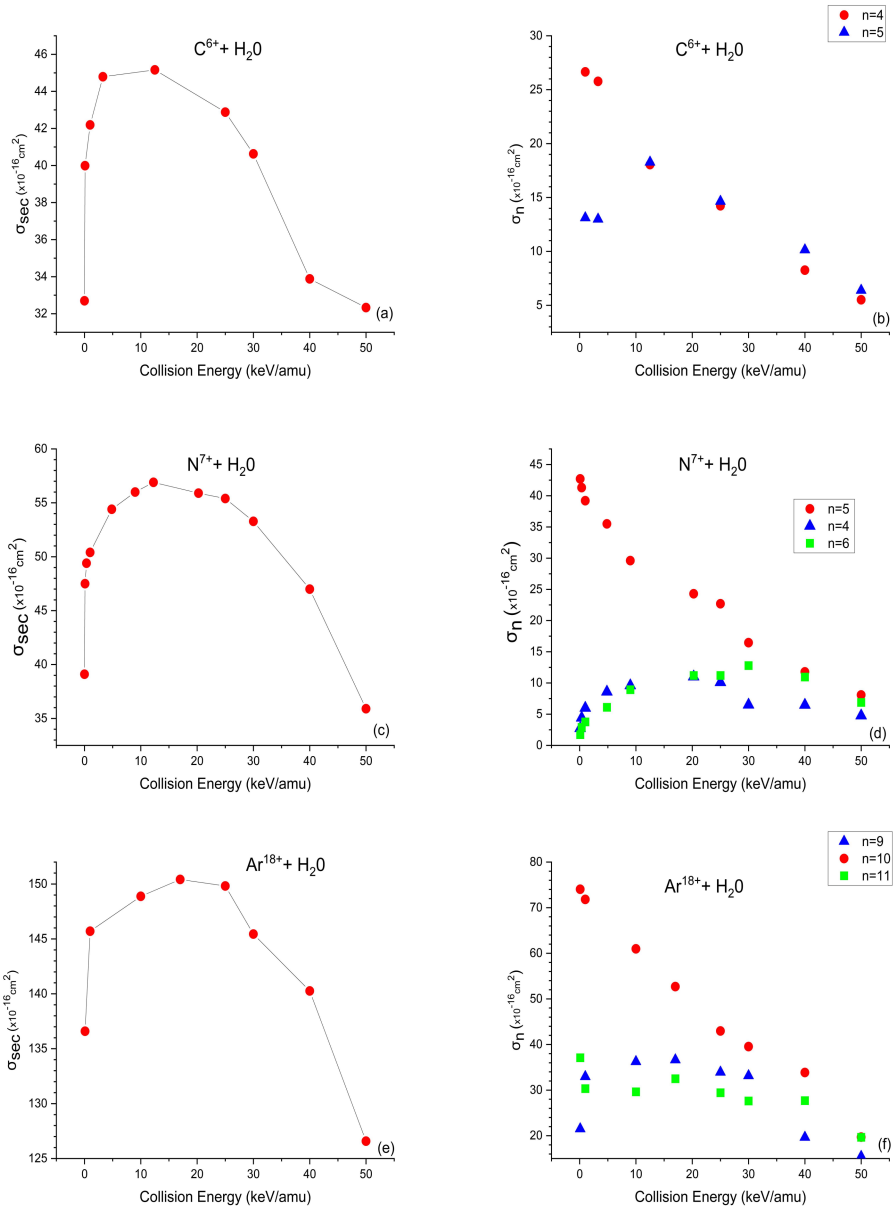

Figure 3. Overall single-electron capture cross sections and the state-specific cross sections for the most prominent principal quantum numbers of the captured electrons for C^{6+} (**a**,**b**), N^{7+} (**c**,**d**), and Ar^{18+} (**e**,**f**), for energies ranging from 10 eV/amu to 50 keV/amu.

We calculated the state-specific capture cross sections for 12 collision energies ranging from 0.01 keV/amu to 20.25 keV/amu, as explained in the theoretical method section above, and assigned each cross section a weight based on its collision energy value on the M-B distribution. The resultant state-specific cross section is then found by

$$\sigma_n = \sum_{i=1}^{12} \propto_i \sigma_{i,n}, \tag{8}$$

where $\propto_i$ is the weight factor and $\sigma_{i,n}$ is the state-specific cross section associated with collision energy E_i.

The results are shown in Table 1. The results labeled NewCTMC are from this work. The results labeled CTMC by Hasan et al. [23] were obtained assuming the active electron is in a 2p atomic orbital around an oxygen ion with an effective charge of $Z = 1$, an electron

binding energy of 12.62 eV, and radial and momentum distributions identical to those shown in Figure 1.

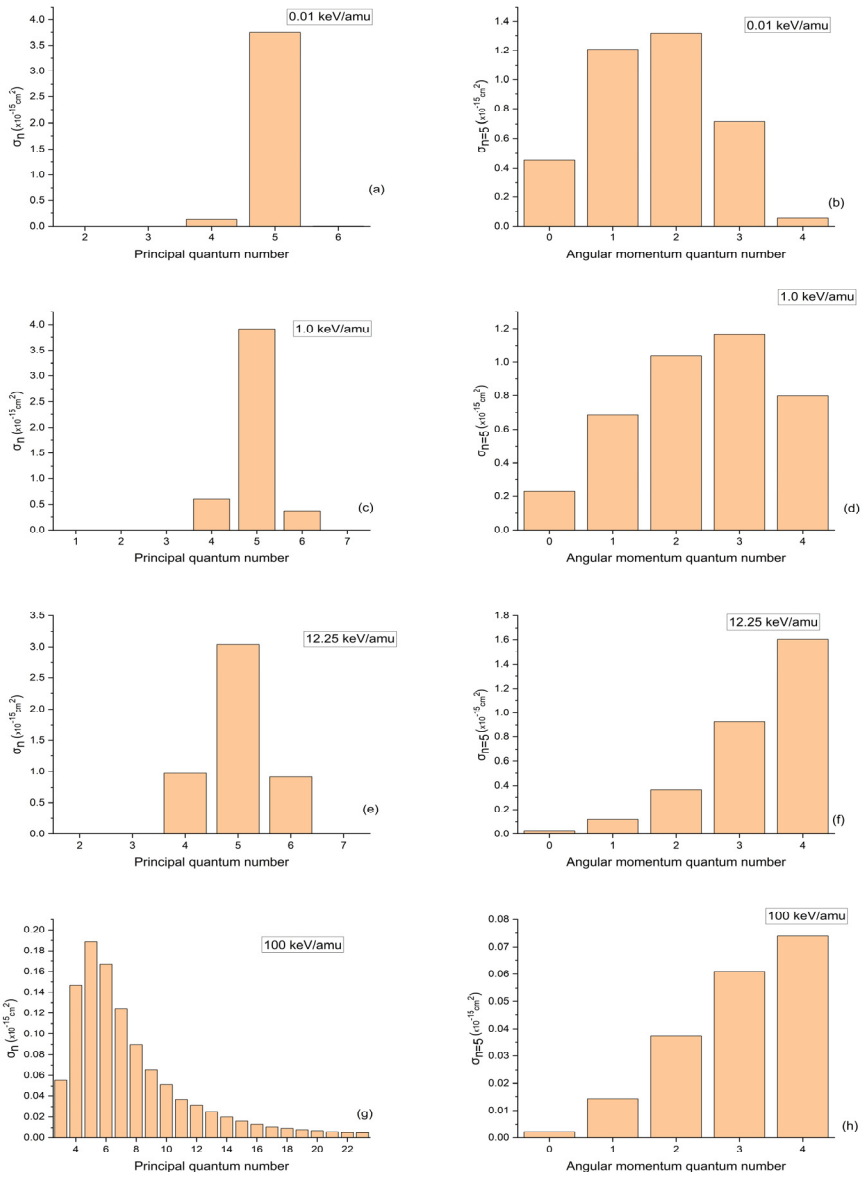

Figure 4. Histograms for the principal quantum numbers populated by the captured electrons in collisions between N^{7+} and H_2O at energies of 100 eV/amu, 1 keV/amu, 12.25 keV/amu, and 100 keV/amu (**a**,**c**,**e**,**g**). Also shown are the angular-momentum quantum states populated by the electrons captured into the $n = 5$ state (**b**,**d**,**f**,**h**).

Both CTMC methods predict the trend that capture proceeds into a narrow range of n-levels at low collision energies, but the method used in this study outperforms the regular CTMC method when comparing the percentage of captures into specific principal quantum states with experimental measurements. This difference between the methods is also reflected in the average principal quantum states occupied, as shown in the table. The overall single-electron capture cross section from NewCTMC is smaller than the CTMC results as well as those from the experimental results of Greenwood et al. [24]. One reason may be that our NewCTMC method does not include multielectron processes that can lead to single-charge exchange, which is clearly observed in the experimental results.

Table 1. Absolute single-electron capture (σ_{sec}) and relative state-selective (σ_n) capture cross sections.

Study	σ_4 (%)	σ_5 (%)	σ_6 (%)	Avg. n	σ ($\times 10^{-15}$ cm^2)
2 keV/amu on H_2O					
Exp.(N^{7+}) [a]	11.5 ± 0.1	87.6 ± 0.1	0.8 ± 0.1	4.89	9.5 [b] (3.27 keV/amu)
Exp.(O^{7+}) [a]	13.5 ± 1.2	85.1 ± 2.4	1.4 ± 0.7	4.88	5.3 [b] (2.72 keV/amu)
CTMC [c]	36	56	4	4.58	9
NewCTMC	13.4	71	9.6	4.93	5.3
4.67 keV/amu on H_2O					
Exp.(N7) [a]	17.1 ± 0.2	73.4 ± 0.3	9.5 ± 0.2	4.92	
CTMC [c]	34	53	7	4.52	9
NewCTMC	14	70	10	4.95	5.3

The CTMC and NewCTMC results are for N^{7+} projectiles. [a] Experimental results from Hasan et al. [23]. [b] Experimental results for single-electron capture cross sections from Greenwood et al. [24]. [c] Calculation from Hasan et al. [23] assumes the target is oxygen with a 2p electron.

Experimental results for both N^{7+} and O^{7+} projectiles are shown. Our NewCTMC method does not distinguish between the two because our calculated single-electron capture cross sections depend on the projectile charge, target electron binding energy, and collision energies, but not on multiple-electron interactions.

4. Conclusions

We have used a classical trajectory Monte Carlo method to model single-electron capture by the bare ions C^{6+}, N^{7+}, Ne^{10+}, and Ar^{18+} from H_2O, modifying the method to match the momentum distribution of the molecule's orbitals as determined using a wavefunction that assumes a single target center. The effective charge of the single-center molecule was chosen to minimize variance between the radial distribution of the CTMC model and the quantum radial distribution.

Absolute single-electron capture cross sections were reported for collision energies ranging from 10 eV/amu to 50 keV/amu. Cross sections for capture into the most populated principal quantum states, as well as the angular-momentum quantum states, were also reported.

Our results show that for all cases, when the collision energy is below 10 keV/amu, only one or two principal quantum states are populated during capture, and these can be predicted using the known scaling rule.

Because conservation of angular momentum is an inherent feature of this method, it can be used to estimate hardness ratios for single-electron capture. We find that capture into the $\boldsymbol{l = 1}$ and $\boldsymbol{l = 2}$ quantum states increases significantly as the collision energy decreases to below 10 keV/amu.

We also made comparisons between experiments for single-electron capture and this CTMC method. The results of these comparisons indicate that this particular method has the potential to be used to estimate the ratio of capture into specific n-states. We find that capture by N^{7+} mostly populates the $\boldsymbol{n = 5}$ state, with the average $\boldsymbol{n}$ being slightly less than 5 due to some capture into the $\boldsymbol{n = 4}$ state, in agreement with experiments.

This method appears to be a promising approach for estimating state-specific capture cross sections at the low collision energies required for modeling X-ray and EUV emissions resulting from collisions between highly charged ions and atoms or molecules of astrophysical interest. In the future, we plan to include the possibility of double capture followed by Auger emission in our single-electron capture model. Comparisons with other

experimental state-selective cross sections and EUV emission measurements [25,26] should allow us to adjust and improve the method.

Author Contributions: Both authors contributed to the calculations, figures, and analysis presented in this work. J.A.P. is responsible for writing of the bulk of the paper. All authors have read and agreed to the published version of the manuscript.

Funding: This research received no external funding.

Data Availability Statement: Data are contained within the article.

Acknowledgments: This research was made possible by funding from the Luther College Office of the Provost.

Conflicts of Interest: The authors declare no conflicts of interest.

Abbreviations

The following abbreviations are used in this manuscript:

AMU	Atomic Mass Unit
CTMC	Classical Trajectory Monte Carlo
EUV	Extreme Ultraviolet
SEC	Single-Electron Capture

References

1. Lisse, C.M.; Dennerl, K.; Englhauser, J.; Harden, M.; Marshall, F.E.; Mumma, M.J.; Petre, R.; Pye, J.P.; Ricketts, M.J.; Schmitt, J.; et al. Discovery of X-ray and Extreme Ultraviolet Emission from Comet C/Hyakutake 1996 B2. *Science* **1996**, *274*, 205–209. [CrossRef]
2. Lisse, C.M.; Christian, D.J.; Dennerl, K.; Meech, K.J.; Petre, R.; Weaver, H.A.; Wolk, S.J. Charge Exchange-Induced X-Ray Emission from Comet C/1999 S4 (Linear). *Science* **2001**, *292*, 1343–1348. [CrossRef] [PubMed]
3. Lisse, C.M.; Dennerl, K.; Englhauser, J.; Trümper, J.; Marshall, F.E.; Petre, R.; Valinia, A.; Kellett, B.J.; Bingham, R. X-Ray Emission from Comet Hale-Bopp. *Earth Moon Planets* **1997**, *77*, 283–291. [CrossRef]
4. Lisse, C.M.; Christian, D.; Dennerl, K.; Englhauser, J.; Trümper, J.; Desch, M.; Marshall, F.E.; Petre, R.; Snowden, S. X-Ray and Extreme Ultraviolet Emission from Comet P/Encke 1997. *Icarus* **1999**, *141*, 316–330. [CrossRef]
5. Dennerl, K.; Englhauser, J.; Trümper, J. X-Ray Emissions from Comets Detected in the Röntgen X-ray Satellite All-Sky Survey. *Science* **1997**, *277*, 1625–1630. [CrossRef]
6. Krasnopolsky, V.A.; Mumma, M.J. Spectroscopy of Comet Hyakutake at 80-700 Å: First Detection of Solar Wind Charge Transfer Emission. *Astrophys. J.* **2001**, *549*, 629–634. [CrossRef]
7. Cravens, T.E. Comet Hyakutake x-ray source: Charge transfer of solar wind heavy ions. *Geophys. Res. Lett.* **1997**, *24*, 105–108. [CrossRef]
8. Häberli, R.M.; Gambosi, T.I.; De Zeeuw, D.L.; Combi, M.R.; Powell, K.G. Modeling of Cometary X-rays Caused by Solar Wind Minor Ions. *Science* **1997**, *276*, 939–942. [CrossRef]
9. Schwadron, N.A.; Cravens, T.E. Implications of Solar Wind Composition for Cometary X-Rays. *Astrophys. J.* **2000**, *544*, 558–566. [CrossRef]
10. Kharchenko, V.; Rigazio, M.; Dalgarno, A. Charge Abundances Of The Solar Wind Ions Inferred From Cometary X-Ray Spectra. *Astrophys. J.* **2003**, *585*, L73–L75. [CrossRef]
11. Beiersdorfer, P.; Olson, R.E.; Brown, G.V.; Chen, H.; Harris, C.L.; Neill, P.A.; Schweikhard, L.; Utter, S.B.; Widmann, K. X-ray Emission Following Low-Energy Charge Exchange Collisions of Highly Charged Ions. *Phys. Rev. Lett.* **2000**, *24*, 5090–5093. [CrossRef]
12. Olson, R.E. n, l distributions in Aq+ + H electron capture collisions. *Phys. Rev. A* **1981**, *24*, 1726–1733. [CrossRef]
13. Janev, R.K.; Belkić, D.S.; Bransden, B.H. Total and partial cross sections for electron capture in collisions of hydrogen atoms with fully stripped ions. *Phys. Rev. A* **1983**, *28*, 1293–1302. [CrossRef]
14. Perez, J.A.; Olson, R.E.; Beiersdorfer, P. Charge transfer and x-ray emission reactions involving highly charged ions and neutral hydrogen. *J. Phys. B At. Mol. Opt. Phys.* **2001**, *34*, 3063–3072. [CrossRef]
15. Salop, A.; Olson, R.E. Charge exchange between H(1s) and fully stripped heavy ions at low-keV impact energies. *Phys. Rev. A* **1976**, *13*, 1312–1320. [CrossRef]

16. Olson, R.E. Classical Trajectory and Monte Carlo Techniques. In *Atomic, Molecular, and Optical Physics Handbook*; Drake, G.W.F., Ed.; American Institute of Physics: New York, NY, USA, 1996; pp. 664–668.
17. Garvey, R.H.; Jackman, C.H.; Green, A.E.S. Independent-particle-model potentials for atoms and ions with 36 < Z < 54 and a modified Thomas-Fermi atomic energy formula. *Phys. Rev. A* **1975**, *12*, 1144–1152.
18. Becker, R.L.; MacKellar, A.D. Theoretical initial l dependence of ion-Rydberg-atom collision cross sections. *J. Phys. B At. Mol. Phys.* **1984**, *17*, 3923–3942. [CrossRef]
19. Moccia, R. OneCenter Basis Set SCF MO's. III. H_2O, H_2S, and HCL. *J. Chem. Phys.* **1964**, *40*, 2186–2192. [CrossRef]
20. Hardie, D.J.W.; Olson, R.E. Charge transfer and ionization processes involving multiply charged ions in collision with atomic hydrogen. *J. Phys. B At. Mol. Phys.* **1983**, *16*, 1983–1996. [CrossRef]
21. Cariatore, N.D.; Otranto, S.; Olson, R.E. Classical description of H(1s) and H*(n=2) for cross section calculations relevant to charge exchange calculations. *Phys. Rev. A* **2015**, *91*, 042709. [CrossRef]
22. Otranto, S.; Olson, R.E. Charge exchange and x-ray emission cross sections for multiply charged ions colliding with H_2O. *Phys. Rev. A* **2008**, *77*, 022709. [CrossRef]
23. Hasan, A.A.; Eissa, F.; Ali, R.; Stancil, P.C. State-Selective Charge Transfer Studies Relevant to Solar Wind-Comet Interactions. *Astrophys. J.* **2001**, *560*, L201–L205. [CrossRef]
24. Greenwood, J.B.; Williams, I.D.; Smith, S.J.; Chutjian, A. Experimental investigation of the process determining x-ray emission intensities from charge exchange collisions. *Phys. Rev. A* **2001**, *63*, 062707. [CrossRef]
25. Bodewits, D.; Hoekstra, R. Electron capture in collisions between O^{6+} ions and H_2O molecules. *Phys. Rev. A* **2007**, *76*, 032703. [CrossRef]
26. Bodewits, D.; Hoekstra, R. Charge-Exchange Emission from Hydrogen-like Carbon Ions Colliding with Water Molecules. *Atoms* **2019**, *7*, 17. [CrossRef]